2021 43rd Annual International Conference of the
IEEE Engineering in Medicine & Biology Society (EMBC)
Oct 31 - Nov 4, 2021. Virtual Conference

Frequency-Time Domain (FTD) Impedance Data Analysis to Improve Accuracy of Microparticle Enumeration in a Microfluidic Electronic Counter

Brandon K. Ashley, and Umer Hassan, *Member, IEEE*

Abstract— **Experimental background noise present in biosensors' data hinders the ability for sensitive and accurate detection of critical biomarkers. Here, we report our digital signal processing analysis with respect to frequency and time domain (FTD) data to reduce noise in an experimental microfluidic impedance cytometer. We evaluated the effectiveness of employed noise filtering techniques independently, including baseline drift correction, high frequency noise filtering, and powerline interference mitigation. We further explored the combined effect of all filters and determine improvements in signal-to-noise (SNR) ratio and particle counting accuracy. By removing noise regimes, SNR improved with this impedance cytometer device, and our future efforts will explore filtering effects of more specific and uncommon noise spectrums to greater optimize device performance.**

I. Introduction

The field of biosensors has grown significantly in the past 20 years, and now provides a myriad of detection options including optical/fluorescence imaging [1], electrically-based [2]–[4], acoustics [5], and many more. Throughout all of them though is the need for identifying desired signal and isolating it from background noise. This noise can arise from environmental factors, intrinsic artifacts from the equipment used, or competing off-target analytes persistent in the sample [6], [7]. Reducing noise and improving the signal sensitivity measured by the signal-to-noise ratio (SNR) is vital for robust and accurate biosensor performance.

Some techniques include improving equipment acquisition or modifying sample preparations [8]. For many optimized cases, however, the most robust option is digital data processing and noise filtering post data collection [9]. This is performed by interpreting the collected values in the frequency or Fourier domain. Here, data is transformed into a series of waveforms that are categorized by frequency and the prevalence of those frequencies are represented in a distribution. While a useful technique for known noise and signal regimes, the interlacing which can occur between them reduces the frequency domain role as only observational.

Here, we present a stepwise digital signal processing approach for improving SNR in an impedance-based microfluidic biosensor through assessments of frequency and time domain (FTD) data. We have designed and fabricated a microfluidic device using gold electrodes to count 9 μm polystyrene particles, representing immune cells based on relative size which are useful for diagnosing cancer [10], HIV [11], diabetes [12], and more. After retrieving bipolar pulses, we introduce a series of digital filters by isolating specific noise regimes which arise from signal baseline drift, high frequency dependencies, and powerline interference (PLI) [13], [14]. While some of these approaches have been used, to the best of our knowledge this is the first time these noise reduction approaches have been evaluated and applied together in a real-sample impedance cytometry apparatus.

Research supported by the National Institute of Health T32 GM135141 and the National Science Foundation Grant Number 2053149.

B .K. Ashley is with the Department of Biomedical Engineering at Rutgers, the State University of New Jersey, Piscataway, NJ 08854 USA.

U. Hassan is with the Department of Biomedical Engineering, the Department of Electrical Engineering, and the Global Health Institute at Rutgers, the State University of New Jersey, Piscataway, NJ 08854 USA (phone: 1-848-4452164, email: umer.hassan@rutgers.edu).

II. Materials and Methods

A. Materials

9 μm polystyrene (PS) particles (2.5% w/v) were purchased from Spherotech (Lake Forest, USA), Sylgard 184 was purchased from Dow (Midland, USA), phosphate buffered saline (PBS, 1X) was purchased from Thermo Fisher Scientific (Waltham, USA), 4" borosilicate and silicon wafers were purchased from University Wafer (South Boston, USA), photoresist was purchased from Kayakuam (Tokyo, JPN), epoxy adhesive was purchased from Digi-Key Electronics (Thief River Falls, USA), and (3-Amino-propyl)triethoxysilane (APTES) was purchased from Sigma Aldrich (St. Louis, USA). Printed circuit boards (PCBs) were purchased from Sunstone Circuits (Mulino, USA), HF2TA Current and Lock-in Amplifiers were purchased from Zurich Instruments (Zurich, SUI). A PCIe-6361 (16 bit, 2 MS/s) data acquisition card and LabView software were purchased through National Instruments (Austin, USA). MATLAB was purchased through MathWorks (Natick, USA).

B. Gold Electrode and Microfluidic Channel Fabrication

Microposit s1813 photoresist was spin-coated above a 4" borosilicate wafer (1.55 μm layer). SU-8 3025 photoresist was spin-coated above a 4" silicon wafer (22 μm layer). For both, photolithography is performed per the manufacturer's protocol. The borosilicate wafer is sputtered with 250 nm of chromium and 750 nm of gold. After liftoff, individual devices are cut out with a diamond saw (Fig. 1a). The silicon wafer surface is treated with ATPES. PDMS is formed by combining 10 parts Sylgard 184 elastomer base with 1 part curing agent and cured over the silicon wafer. After curing, PDMS is removed, and inlet and outlet holes are punched.

C. Microfluidic Device Connection and Interfacing

The PDMS channel and gold electrodes are treated with oxygen plasma using a plasma chamber (100W power for 1 min at 60 cm^3/min of O_2). Immediately after, the PDMS is

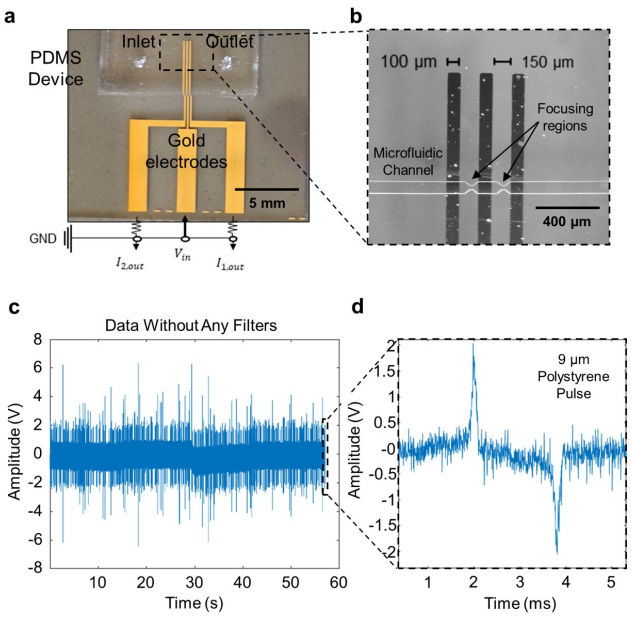

Figure 1. a) Image of gold microelectrodes bonded with PDMS microfluidic device. b) Microscope image of electrode sensing region, with electrode alignment between channel focusing regio\ns. c) Time domain impedance results for 9 µm polystyrene particles flowing through device. d) Enhanced bipolar pulse to obersve peak amplitude compared to noise.

aligned and bonded above the microelectrodes with focusing regions positioned between outer electrodes (Fig. 1b). Syringe tubing was inserted into PDMS inlet and outlet holes to facilitate media flow using a syringe pump.

Silver conductive epoxy connects the microfluidic devices with a custom PCB. The PCB then connects with a custom Veroboard which facilitates transimpedance amplification for signal detection using HF2TA current amplifiers from outer electrodes and inputs a 5V AC signal to the middle electrode using a lock-in amplifier (Fig. 1a). 9 µm PS particles are diluted in 1X PBS at a concentration of $2x10^5$ particles/mL and flow through the device at a 15 µL/min flow rate.

D. Signal Acquisition

Current is received from electric field changes in the microfluidic channel at a 250 kHz sampling rate. This is converted to voltage with a transimpedance amplifier and multiplies the signal with a gain of 1,000. The voltage signals are then combined in a differential amplifier, which changes the results from two separate signals to the difference between them and forms the bipolar signal pulse for the objects passing over the device (Fig. 1c and 1d). This removes common-mode noise that may persist in the circuit.

E. Digital Signal Processing and Sampling Algorithm

Time-domain signals are saved through a LabView control program. A MATLAB algorithm sets a threshold of values greater than 5x the background noise to indicate PS particle detection. Here, background noise (σ_{BG}) is the root means squared (rms) of 5,000 data points without particle pulses ($data_{noise}$) after manually visualizing the data (Eq. 1):

$$\sigma_{BG} = \text{rms}(data_{noise}) \quad (1)$$

Bipolar amplitude for one particle (ΔV_T) is measured as the maximum value (ΔV_{max}) minus the minimum (ΔV_{min}) for 500 data points ± the threshold position, shown by Eq. 2:

$$\Delta V_T = \Delta V_{max} - \Delta V_{min} \quad (2)$$

To ignore two or more PS particles flowing through the electric field at once, bipolar amplitudes are binned into 6 discrete categories, and the most common category is selected as one particle flowing through the channel ($\Delta E_{T,1\ particle}$). The SNR is calculated using this signal mode (Eq. 3):

$$SNR = 20\log_{10}(\text{rms}(\Delta V_{T,1\ particle})/\sigma_{BG}) \quad (3)$$

Subsequent digital filters are applied using MATLAB. A 4th order Butterworth filter is used for high and low pass filters, while a 1st order Butterworth filter is used for the band-stop filters using the Signal Processing Toolbox. Signals are converted from time-domain to frequency-domain values using the fast Fourier transform (FFT) function in MATLAB.

III. Results and Discussion

A. Original Unprocessed Data

After magnifying signal acquired using transimpedance current amplifiers, Fig. 1c represents the raw data without post processing or frequency analysis, with a bipolar pulse recorded over time (Fig. 1d). From this, there are several noticeable signal restrictions including voltage drift and a large persistent noise band. There are also incidences of larger particle amplitudes, which may be attributed to two or more particles being detected at once. This theory is supported by the fact that most particle peaks are divisible by the bipolar signal amplitude that occurs most often (2.627±0.313 V). This is quantified in Table 1, along with metrics from each filtering effect which will be discussed later. After visualizing signal spectra in the frequency domain (Fig. 2a)

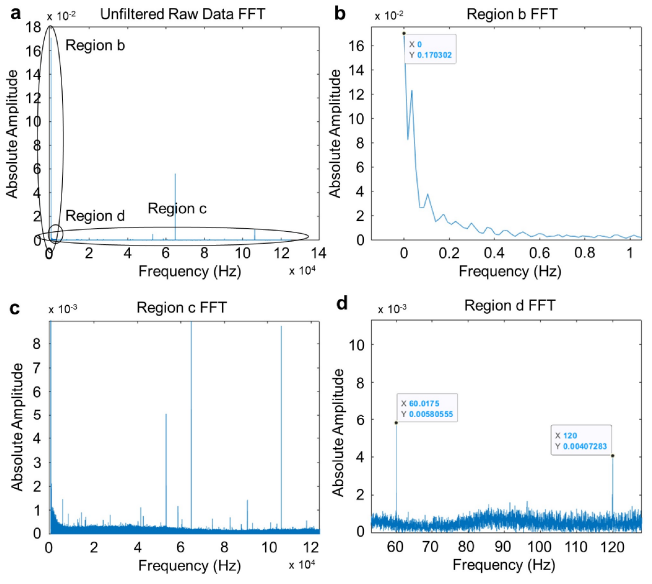

Figure 2. a) Fourier transform (FFT) showing frequency domain results of unfiltered raw data. b) Expanded low frequency region to highlight high amplitude baseline drift. c) Expanded low amplitude region to better visualize frequency distribution. d) Expanded plot to show powerline interference frequency visualizaition at 60 and 120 Hz.

using Fourier transform (FFT) analysis, many large amplitudes occur at low frequencies shown in Region b (Fig. 2b) with a few exceptions. When focusing to view amplitude distribution across all frequencies (Fig. 2c), there is a general baseline amplitude up to 120 kHz produced by a combination of data related to both particle impedance detection and background noise. As further filtering effects are explored, it will be revealed which frequency regimes are attributed to particle peaks and which can be removed to reduce background noise and improve signal quality.

B. Filtering Powerline Interference (PLI) Frequencies

The sharp amplitudes that arise from the 60 and 120 Hz frequencies are used in power supplies for electrical equipment in the U.S, which uses a standard 120V AC voltage input at a 60 Hz frequency that persists through to measurements in the device. Additionally, the voltage source has significant amplitude at the second harmonic of its frequency at 120 Hz. While other peaks are seen at further harmonics (180 Hz, 240 Hz, etc.) their relative amplitudes are negligible as harmonic persistence diminishes relative to the original frequency. As such, values related to 60 and 120 Hz are predominantly the result of this electric source known as powerline interference (PLI) which is entirely noise.

To overcome PLI, band-stop filters were implemented which selected and attenuated data from frequencies between 59.5-60.5 Hz and 119.5-120.5 Hz. Fig. 3 shows the FTD result of these efforts. While little difference can be observed by visualizing the time-domain data (Fig. 3a) versus no data processing, in the frequency domain the PLI frequencies were negated by the band-stop filter (Fig. 3b). As particle pulse frequencies may be above 50 Hz, this tight range for PLI removal was to prevent particle signal degradation, and the first-order filter was still satisfactory in powerline attenuation. After recording particle pulses and measuring noise (Table 1), there is slightly improved signal quality (23.741±0.189 dB SNR with PLI removed vs. 23.732±0.380 dB SNR for raw data). Nonetheless, the effects of PLI are constant in the U.S. regardless of device voltage input, user-defined frequency input, sampling rate, or media flow rate, and as such should be included to mitigate potential signal loss over different parameters.

C. Filtering High Frequency Data

As PS particles pass through the electric field, their recorded peak has a consistent width that is based on the transit time across this distance. With a flow rate of 15 µL/min for these experiments, these bipolar pulses and

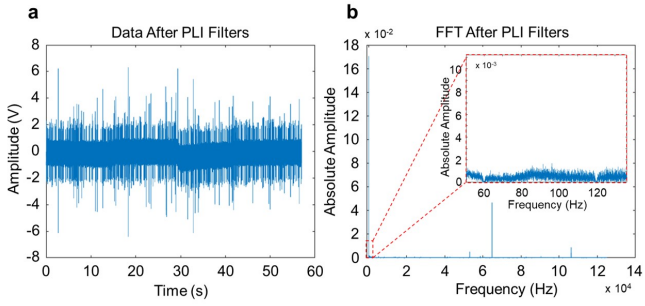

Figure 3. a) Time domain for 9 µm polystyrene particles after only removing powerline interference using band-stop filters. b) Fourier transform (FFT) showing frequency domain results of data, with insert revealing the removed peaks at 60 Hz and the 120 Hz second harmonic.

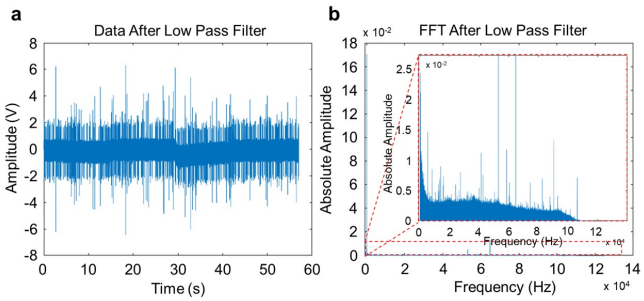

Figure 4. a) Time domain for 9 µm polystyrene particles after only removing frequencies above 100 kHz using a low pass filter. b) Fourier transform (FFT) showing frequency domain results of data, with frequency amplitude falling off after 100 kHz as highlighted in the expanded insert.

attributed data are found within a frequency regime between 50 Hz and 90 kHz [9], and thus higher frequency domains hold primarily noise data. By applying a low pass filter alone to reduce amplitudes above 100 kHz, overall background noise was reduced. Fig. 4a visualizes this, as the noise band throughout the time domain data is thinner, and the insert graph in Fig. 4b confirms a steady amplitude drop-off for frequencies greater than 100 kHz due to the low-pass filter. This is further quantified in Table 1, where noise is lower, and SNR increased more than filtering PLI alone (Table 1). Frequencies above 100 kHz may represent the most widespread noise-only regime in the Fourier domain, but further filtering can isolate and remove the largest amplitude noise present at low frequencies.

D. Filtering Low Frequency Data

The largest amplitude in the Fourier domain is attributed to background noise. Indeed, frequencies below 20 Hz represents the baseline drift which is the result of external ionization from external electrical equipment and minor flow variances [6]. Quantization may manifest in baseline drift as well but is negligible in relation to external factors as a high bitrate is used in the data acquisition card. This drift is a significant limitation as it alters the range particle pulses are detected with the same amplitude from its cutoff point, resulting in inaccurate particle counting with false negatives. While many complicated techniques have been employed to remove baseline drift [15], if the desired signal is not in the baseline drift regime then the simplest method of a well-selected high pass filter is most appropriate [13].

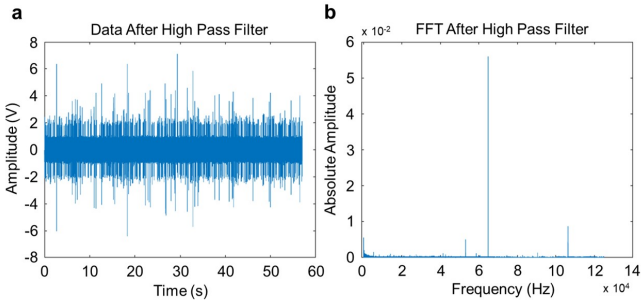

Figure 5. a) Time domain for 9 µm polystyrene particles after only removing frequencies below 20 Hz using a high pass filter. b) Fourier transform (FFT) showing frequency domain results of data, with signals below 20 Hz significantly negated.

TABLE I. SIGNAL RETRIVAL FROM FILTERING EFFECTS

Filter Applied	*Noise (σ_{BG}, V)*	*Signal Mode (V)*	*Signal-to-Noise Ratio (SNR, dB)*
No Filter	0.1709	2.627±0.117	23.732±0.380
PLI[a]	0.1707	2.626±0.058	23.741±0.189
Low Pass (100 kHz)	0.1596	2.638±0.052	24.364±0.171
High Pass (20 Hz)	0.1708	2.946±0.056	24.736±0.164
All Filters	0.1531	2.854±0.053	25.409±0.159

a. PLI = Powerline Interference (Band-stop filters at 60 and 120 Hz)

Fig. 5 represents FTD results after applying a high pass filter alone. The most apparent change is the time domain data is normalized to 0V and drift is removed (Fig. 5a), while low frequency data is removed in the FFT domain (Fig. 5b). While persistent noise amplitude does not appear to change in magnitude, this filter improves PS pulse detection by increasing their average amplitude. Concurrently, SNR increases, and PS pulses are more identifiable (Table 1).

E. Effects of Combined Filtering

Finally, the use of a low pass filter, high pass filter, and band-stop filters to eliminate PLI were used in series to evaluate synergistic properties in ameliorating SNR. Fig. 6 details these results, which affirms the added effects of removing baseline drift with reducing the persistent noise band (Fig. 6a). In the frequency domain (Fig. 6b), the bulk amplitudes are observable without focusing in on any regimes, indicating the largest frequency amplitudes found in the unfiltered signal were the result of all or mostly noise. This also revealed the largest increase in SNR (Table 1), as bipolar amplitude increased from better acquisition after baseline drift was removed and noise was lower comparable to the low pass filter removing high frequency noise.

IV. CONCLUSION

The presented study has detailed iterative effects from digital filtering to reduce biosensor noise and presents the practical application of FTD analysis for experimental impedance data. While SNR improved through these efforts, the final SNR magnitude with all filters applied is relatively small, a consequence of the device's design and the prevalence of common noise. Additionally, the purposed filtering strategies may have less impact for systems which measure biomarkers in different frequency spectra. However, the 9 µm PS particles are the same physical scale to human immune cells, and the device's sensitivity in measuring these particles lends to the possible application of this device in point-of-care cell counting, and biological samples are currently being investigated. Future efforts used alongside FTD can facilitate greater biosensor performance such as machine learning, adaptive filtering, and signal averaging to further define and eliminate noise regimes. As the frequency domain is continuously becoming more understood in relation to signal vs. noise data, future studies may develop an improved biomarker quantification scheme measured entirely from the frequency space.

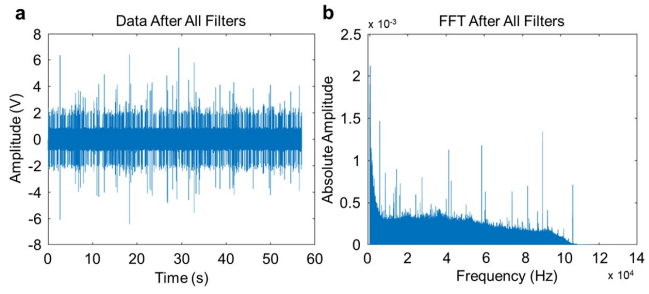

Figure 6. a) Time domain for 9 µm polystyrene particles after applying all filters (20 Hz high pass, 100 kHz low pass, 60 and 120 Hz band-stop filters). b) Fourier transform (FFT) showing all frequency amplitudes after filtering were reduced for common frequencies related to background noise.

REFERENCES

[1] J. P. Houston, M. A. Naivar, and J. P. Freyer, "Digital analysis and sorting of fluorescence lifetime by flow cytometry," *Cytometry Part A*, vol. 77A, no. 9, pp. 861–872, 2010.

[2] X. Liu, L. Li, and A. J. Mason, "High-throughput impedance spectroscopy biosensor array chip," *Philosophical Transactions of the Royal Society A: Mathematical, Physical and Engineering Sciences*, vol. 372, no. 2012, p. 20130107, Mar. 2014.

[3] S. Prakash, B. K. Ashley, P. S. Doyle, and U. Hassan, "Design of a Multiplexed Analyte Biosensor using Digital Barcoded Particles and Impedance Spectroscopy," *Scientific Reports*, vol. 10, no. 1, Art. no. 1, Apr. 2020.

[4] D. D. Stupin, S. V. Koniakhin, N. A. Verlov, and M. V. Dubina, "Adaptive Filtering to Enhance Noise Immunity of Impedance and Admittance Spectroscopy: Comparison with Fourier Transformation," *Phys. Rev. Applied*, vol. 7, no. 5, p. 054024, May 2017.

[5] F. Khateib, A. Mehaney, R. M. Amin, and A. H. Aly, "Ultra-sensitive acoustic biosensor based on a 1D phononic crystal," *Phys. Scr.*, vol. 95, no. 7, p. 075704, May 2020.

[6] K. M. Pierce, B. A. Parsons, and R. E. Synovec, "Chapter 10 - Pixel-Level Data Analysis Methods for Comprehensive Two-Dimensional Chromatography," in *Data Handling in Science and Technology*, vol. 29, A. M. de la Peña, H. C. Goicoechea, G. M. Escandar, and A. C. Olivieri, Eds. Elsevier, 2015, pp. 427–463.

[7] M. R. Ram, K. V. Madhav, E. H. Krishna, N. R. Komalla, and K. A. Reddy, "A Novel Approach for Motion Artifact Reduction in PPG Signals Based on AS-LMS Adaptive Filter," *IEEE Transactions on Instrumentation and Measurement*, vol. 61, no. 5, pp. 1445–1457, May 2012.

[8] K. Ridgway, S. P. D. Lalljie, and R. M. Smith, "Sample preparation techniques for the determination of trace residues and contaminants in foods," *Journal of Chromatography A*, vol. 1153, no. 1, pp. 36–53, Jun. 2007.

[9] U. Hassan *et al.*, "A microfluidic biochip for complete blood cell counts at the point-of-care," *Technology*, vol. 03, no. 04, pp. 201–213, Dec. 2015.

[10] K. Ahuja *et al.*, "Toward point-of-care assessment of patient response: a portable tool for rapidly assessing cancer drug efficacy using multifrequency impedance cytometry and supervised machine learning," *Microsystems & Nanoengineering*, vol. 5, no. 1, Art. no. 1, Jul. 2019.

[11] N. N. Watkins *et al.*, "Microfluidic CD4+ and CD8+ T Lymphocyte Counters for Point-of-Care HIV Diagnostics Using Whole Blood," *Science Translational Medicine*, vol. 5, no. 214, pp. 214ra170-214ra170, Dec. 2013.

[12] Z. Lu *et al.*, "A point of care electrochemical impedance spectroscopy device," in *2015 28th IEEE International System-on-Chip Conference (SOCC)*, Sep. 2015, pp. 240–244.

[13] A. K. Atakan, W. E. Blass, and D. E. Jennings, "Elimination of Baseline Variations from a Recorded Spectrum by Ultra-Low Frequency Filtering," *Appl Spectrosc*, vol. 34, no. 3, pp. 369–372, May 1980.

[14] U.S. Navy Bureau of Naval Personnel Staff, *Basic Electricity*. New York: Dover Publications, 1970.

[15] V. S. Chouhan and S. S. Mehta, "Total Removal of Baseline Drift from ECG Signal," in *2007 International Conference on Computing: Theory and Applications (ICCTA'07)*, Mar. 2007, pp. 512–515.